International Journal of Nanomedicine

Dovepress
open access to scientific and medical research

Open Access Full Text Article

ORIGINAL RESEARCH

Influence of thermomechanical processing on biomechanical compatibility and electrochemical behavior of new near beta alloy, Ti-20.6Nb-13.6Zr-0.5V

This article was published in the following Dove Press journal:
International Journal of Nanomedicine
1 October 2015
Number of times this article has been viewed

Mohsin Talib Mohammed[1]
Zahid A Khan[1]
Geetha Manivasagam[2]
Arshad N Siddiquee[1]

[1]Mechanical Engineering Department, Faculty of Engineering, Jamia Millia Islamia, New Delhi, [2]Centre for Biomaterials Science and Technology, VIT University, Vellore, India

Abstract: This paper presents the results for the effect of different methods of thermomechanical processing on the mechanical properties and electrochemical behavior of metastable β alloy Ti-20.6Nb-13.6Zr-0.5V (TNZV). The thermomechanical processing included hot working, solution heat treatments at different temperatures, and cooling rates in addition to aging. The thermomechanical processing conditions used in the study resulted in attainment of a wide range of microstructures with varying spatial distributions and morphologies of elongated/equiaxed α, β phases, or martensite, as a result of which several tensile properties were achieved. Aging treatment led to an increase in hardness, elastic modulus, and tensile strength and a decrease in ductility (elongation). Electrochemical tests indicated that the TNZV alloy undergoes spontaneous passivation due to spontaneous formation of an oxide film in the environment of the human body. Because the air-cooled samples possessed high hardness and also a fine grain size, they showed a lower corrosion rate than the samples treated under other conditions.

Keywords: titanium alloys, biomedical applications, mechanical properties, corrosion

Introduction

Engineering materials used in biomedical applications must have optimal mechanical properties and biocompatibility, and should remain chemically stable under severely hostile conditions. In comparison with biomedical stainless steels and cobalt-chromium alloys, titanium (Ti)-based alloys show properties such as low specific strength and excellent resistance to corrosion, as well as a low elastic modulus close to that of bones, so they are the materials of choice for structural biomedical applications.[1–4]

Because of its excellent specific strength, resistance to corrosion, and biocompatible characteristics, the α+β-type Ti-6Al-4V alloy (ASTM F1108) has been used as a structural biomaterial for the manufacturing of orthopedic prostheses and dental implants.[5] However, the alloying elements present in this alloy have their own adverse effects in the biomedical environment. The literature reports that the presence of vanadium (V) ions in human tissues can alter the kinetics of the enzyme activity associated with cells involved in the inflammatory response.[6,7] It has been reported that aluminum (Al) increases the risk of development of Alzheimer's disease.[8] Further, the low elastic modulus of Ti alloys is a major advantage that makes them suitable implant materials for artificial joints (eg, hip, knee, shoulder). The stiffness of the implant materials must essentially be as close as possible to that of the connected bone to facilitate effective transfer of mechanical stress so as to avoid damage to bone cells.[9] A large difference

Correspondence: Mohsin Talib Mohammed
Mechanical Engineering Department, Faculty of Engineering, Kufa University, PO Box 21, Najaf, Iraq
Tel +964 771 063 9272
Fax +964 33 885 2786
Email mohsent123@yahoo.com

between the stiffness of the implant materials and bone may result in osteoporosis or poor osseointergration,[10] which may consequently lead to crack nucleation and eventual failure of the implant.[11] The modulus of the Ti-6Al-4V alloy is approximately 110 GPa,[12] which is considerably higher than that of human bone (10–40 GPa).[13] The high modulus of Ti-6Al-4V is due to an increased volume fraction of the α phase caused by a high Al content.[14]

In recent times, near β-type Ti alloys, containing niobium (Nb) and zirconium (Zr), have attracted considerable attention for orthopedic implant applications owing to their unique combination of good mechanical properties, low elastic modulus, and superior resistance to biocorrosion. It has been reported that the elastic modulus of these alloys can be significantly reduced by adjusting the concentration of β-stabilizing elements.[15–17] In addition, this type of Ti alloys shows evidence of excellent resistance to corrosion in human body fluid. The main reason for this behavior is the formation of a protective hard and tightly adherent oxide film.[18] Therefore, new β-type Ti alloys have been developed using nontoxic and nonallergic elements such as Nb, Zr, and other such elements.[19] It is well known that Nb is a β-stabilizer element that forms a homogenous solid solution with Ti in all kinds of Ti alloys,[20–22] whereas Zr is traditionally deemed to be a neutral element in the α-type and α+β-type alloys. On the other hand, it has been reported that Zr can be treated as a kind of β-stabilizer in the Ti-Nb-Zr alloy system because it not only inhibits α precipitation[23,24] but also considerably reduces the martensitic transformation start temperature.[25,26] In order to develop safe Ti-based alloys for biomedical applications, Nb and Zr are preferably added as they enhance the ability to achieve biological passivity and the ability to reduce the elastic modulus.[27]

In general, thermomechanical processing (TMP) is a metallurgical process through which work hardening and heat treatment processes are integrated into a single process.[28] TMP plays a crucial role in altering a microstructure, leading to outstanding maaterial properties.[29–31] The mechanical properties[32] and corrosion behavior[33] depend strongly on the alloy composition, processing history, and heat treatment conditions. Since near-β Ti alloys respond to thermal treatment and TMP, various microstructural constituents, like size, shape, and amount of the various phases, can be modified by varying the TMP parameters. However, there have been very few reports of the influence of thermal treatment and TMP on the microstructural features of the as-cast Ti-Nb-Zr alloy system, and in turn, of its mechanical and electrochemical behavior. Geetha et al[33] investigated the effect of heat treatment on the corrosion behavior of Ti-13Zr-13Nb alloy in Ringer's solution and found that water-quenched α+β alloys have superior resistance to corrosion owing to a homogeneous distribution of the alloying elements. Studies pertaining to the effect of TMP on the microstructure and mechanical properties of Ti-13Zr-13Nb alloy[34] and the corrosion behavior of this alloy in simulated body fluid[35] report that major results are achieved due to the cooling rate after solution treatment.

In view of the potential advantages offered by biocompatible Ti alloys, a lot of dedicated focused work needs to be carried out by engineers and materials scientists to develop novel Ti alloys with a low elastic modulus and superior electrochemical behavior for biomedical applications. With this in mind, we investigated the effect of TMP on the microstructure, mechanical properties, and corrosion behavior of a novel Ti-20.6Nb-13.6Zr-0.5V (TNZV) alloy.

Materials and methods

The alloy used in the present investigation was prepared by casting of a mixture of sponge Ti, niobium powder, and Zr chips. The TNZV alloy was prepared using the nonconsumable vacuum arc melting technique and supplied in the form of 600 g pancakes. The pancakes were remelted three times to obtain compositional homogeneity. The composition of the alloy was analyzed, and the chemical composition in wt% is given in Table 1.

The as-cast TNZV alloy was thermally treated at 1,000°C for 1 hour for homogenization and then water-cooled. Subsequently, the homogenized samples were subjected to a 10% by forging above the β transition temperature (850°C) and directly subjected to a 25% reduction by rolling at the same temperature and then air-cooled (AC) to room temperature. After complete plastic deformation, the alloy was found to be free from any metal working defects, indicating that the entire metal working process was performed successfully.

The hot deformed TNZV samples were solution-treated at 850°C (above β transus temperature) for 1 hour in a dynamic argon atmosphere and then either water-quenched (WQ), AC, or furnace-cooled (FC). Aging treatment for the WQ samples was done at 500°C for 5 hours. The TMP route for the TNZV alloy is shown schematically in Figure 1.

Table 1 Chemical composition (wt%) of Ti-20.6Nb-13.6Zr-0.5V

Ti (wt%)	Nb (wt%)	Zr (wt%)	V (wt%)	Fe (wt%)
Balance	20.6	13.6	0.5	0.14

Abbreviations: Nb, niobium; Ti, titanium; Zr, zirconium; V, vanadium; Fe, iron.

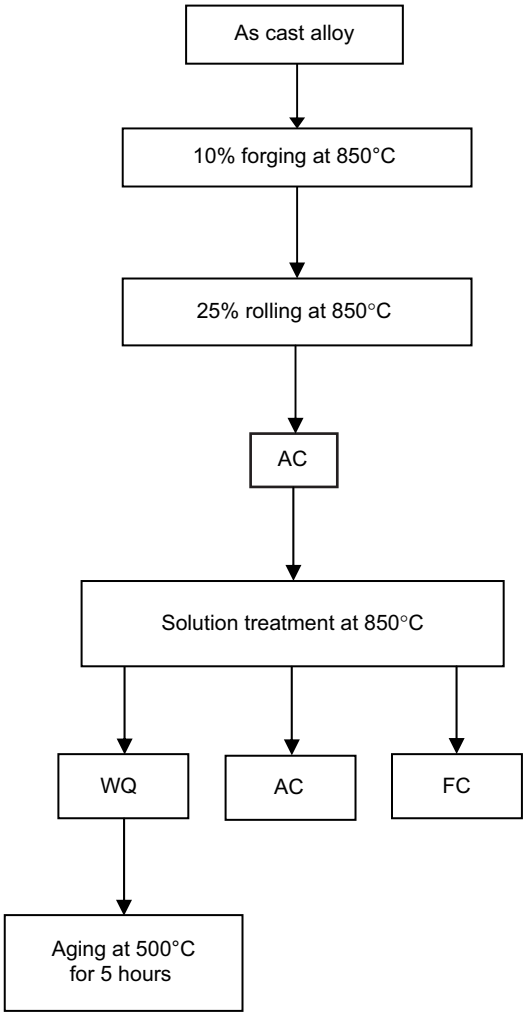

Figure 1 Schematic diagram of the thermomechanical processing of Ti-20.6Nb-13.6Zr-0.5V alloy.
Abbreviations: WQ, water-quenched; AC, air-cooled; FC, furnace-cooled.

The major and trace elements were determined using an X-Strata Isis 1559 X-ray fluorescent spectrometer (Oxford Instruments, Abingdon, UK). Analysis of the microstructure of the thermally treated samples was carried out using an optical microscope and a Nova Nano 450 field emission scanning electron microscope (FEI Company, Eindhoven, The Netherlands) at 2 kV. For microstructural analysis, the metallographic samples were prepared using standard techniques employed for Ti and its alloys.[36] The samples were ground with 1,200 grit silicon carbide, followed by polishing to a mirror finish using 0.5 µm diamond paste. The samples were etched with Kroll's reagent (10 vol% hydrogen fluoride and 5 vol% HNO_3 in water). X-ray diffraction analysis was carried out at room temperature using a PW1830 X-ray diffractometer (Philips, Eindhoven, The Netherlands) with Cu Kα radiation at a wavelength of 1.54056°A at 40 kV and 30 mA. The scanning rate was kept at 3 degrees to 2θ/60 seconds.

Vickers microhardness (HV) measurements were performed on a computer-controlled precision microhardness tester (MicroWhizHard, Mitutoyo Corporation, Kanagawa, Japan) where an indentation load of 300 gf and a dwell time of 5 seconds were used for each of the indents. The HV test was carried out on the polished specimens to obtain a clean and flat surface. Final polishing was carried out using 0.5 µm diamond paste. Ten indentations were taken for each specimen and the average was considered.

Conventional tensile testing was carried out using a computerized UTE-60 universal testing machine (Fuel Instruments & Engineers Pvt Ltd, Kolhapur, India) at a constant cross-head speed of 1 mm per minute in air at room temperature. Mechanical testing, as per ASTM E8M, was performed to determine the ultimate tensile strength (UTS), 0.2% off-set yield strength (YS), and elongation (e%). The elastic modulus was obtained by measuring the slope of the linear part of the stress–strain response. Dog bone-shaped tensile specimens with dimensions as shown in Figure 2 were precisely machined using a wire electrical discharge machine. After machining, tensile specimens were polished using waterproof silicon carbide papers of up to 2,500 grit and the gauge length of the specimens was mechanically polished using 0.5 µm diamond paste.

The corrosion behavior of the TNZV alloy was studied using a potentiostat, comprising a three-electrode cell with Ag/AgCl (KCl saturated) as the reference electrode (all the potential measurements were made with reference to this) and platinum foil as the counter electrode (cathode). Test specimens with dimensions of 10 mm ×10 mm ×2 mm were used as the working electrode (anode). Anodic polarization was carried using a computer-interfaced WPG100e corrosion measuring system and Sequencer version 5 software. The open circuit potential (OCP) and passive current density were used to evaluate the corrosion characteristics of the thermomechanically treated samples of Ti alloy.

The surface area exposed to the electrolyte was 0.126 cm^2. For each experiment, the specimens were prepared by sequential grinding with waterproof emery paper with up to 2,000 grit silicon carbide, followed by polishing with 0.5 µm alumina to obtain a high mirror surface finish, and

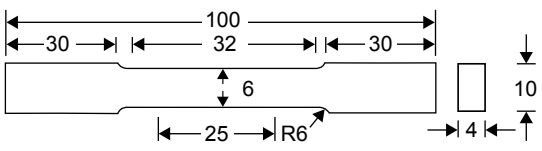

Figure 2 Dimensions of tensile specimen (ASTM E-8 standard).

then cleaning in an ultrasonic bath three times. Freshly prepared Ringer's solution was used as the electrolyte to simulate a body fluid environment.[37–40] This solution when dissolved in 1 L of distilled water had the following chemical composition: 9.00 g NaCl, 0.43 g KCl, 0.20 g $NaHCO_3$, and 0.24 g $CaCl_2$. The pH of the solution was maintained at 7.4. The solution was naturally aerated and kept at 37°C±1°C. The OCP was plotted as a function of time until a stable value was reached. Next, the corrosion potential (E_{corr}) and passive current density (I_{corr}) of the alloy were determined from the potential versus current density polarization curve. The polarization curves were obtained using a scan rate of 0.166 mV per second in the range of 750–2,500 mV (Ag/AgCl). The polarization tests were repeated at least three times for each specimen. The E_{corr} and I_{corr} were determined from the registered curves by the extrapolation method.

Results and discussion

Microstructure and X-ray diffraction analysis

Microstructure and its analysis are important given that several vital characteristics of materials, such as their mechanical and corrosion properties, are strongly influenced by microstructural features. Thermal treatment and TMP are the two main techniques used to achieve the desired microstructure. Microstructure observations of the as-cast sample (Figure 3Aa and Ba) indicated a fine needle-like (acicular) α in the β matrix with segregation of the α phase on grain boundaries. The X-ray diffraction profiles of the as-cast TNZV alloy is shown in Figure 4A, which indicates that only peaks corresponding to the α and β phase are present in the alloy.

The microstructure of the TNZV alloy depends essentially on the plastic deformation process and heat treatment sequences used. Hence, hot working, ie, 10% hot forging plus 25% hot rolling at 850°C (above β transus temperature), is an effective method for generating dynamic recrystallization with an equiaxed structure. It has been observed that treating solution above β transus temperature dissolves the entire α phase developed during hot plastic deformation, leading to complete transformation to β phase in the TNZV alloy. It can be seen from the micrographs in Figure 3Ab, Bb, Ac, and Bc) that hot working and solution treatment at 850°C (above the β transus temperature) led to transformation of a part of β phase to α phase for both FC and AC samples.

In line with the findings of others,[34,41] the microstructure of FC or AC samples consisted of Widmanstätten α-laths (in a basket-weave arrangement) that were composed of different variations of α plates within pre-existing β-grains. The volume fraction of the α phase in the FC samples was high due to the lower cooling rate. The thickness of the α plates in FC samples was higher than that of the AC samples, because the size depended mainly on the cooling rate. Thus, the microstructure of the AC samples shows the presence of fine α-β structures within pre-existing β-grains.

A nonequilibrium metastable martensite phase and a retained β phase were found in the samples which were WQ from solution treatment at 850°C (Figure 3Ad and Bd). A large number of papers have reported the presence of a martensite structure in Ti materials if the solution is treated at a high temperature (above β phase field) with a sufficiently high cooling rate.[20,34,41–46] Thus, rapid cooling from the above temperature resulted in a martensite phase in the microstructure of the WQ samples. Two types of metastable martensites, α′ and α″, which are hexagonal and orthorhombic structures, respectively, are found in Ti alloys quenched from the β phase based on the concentration of the beta alloying elements.[20] In a Ti-Nb binary system, the hexagonal α′ is observed when the Ti alloys contain Nb <13 wt%, whereas the orthorhombic α″ is seen at a higher Nb content.[23,47,48] In the present research, the Nb content in the TNZV was 20.6 wt%, which specifies the formation of orthorhombic α″ martensite after WQ from 850°C. It is reported that the orthorhombic structure of the α″ phase is obtained because of the whole correspondence between the atoms of Ti and Nb associated with the phase change during WQ could result in formation of the orthorhombic α″ phase.[49]

Aging of WQ samples at 500°C for 5 hours is a diffusion-controlled process. During aging, the martensite phase decomposes into the α+β phase structure and generates a fine distribution of small globular α along the pre-existing martensite plates (Figure 3Ae and Be). It is reported that the orthorhombic martensite α″ phase is metastable and transforms to an α+β phase structure if the martensitic transformation start temperature is more than room temperature.[50]

To obtain an indepth understanding, the above phase constituents in the microstructures of the thermally treated TNZV samples were identified using X-ray diffraction spectra as seen in Figure 4B, which shows the presence of peaks of α and β phases in FC, AC, and aged TNZV samples, whereas only martensite is found in WQ samples.

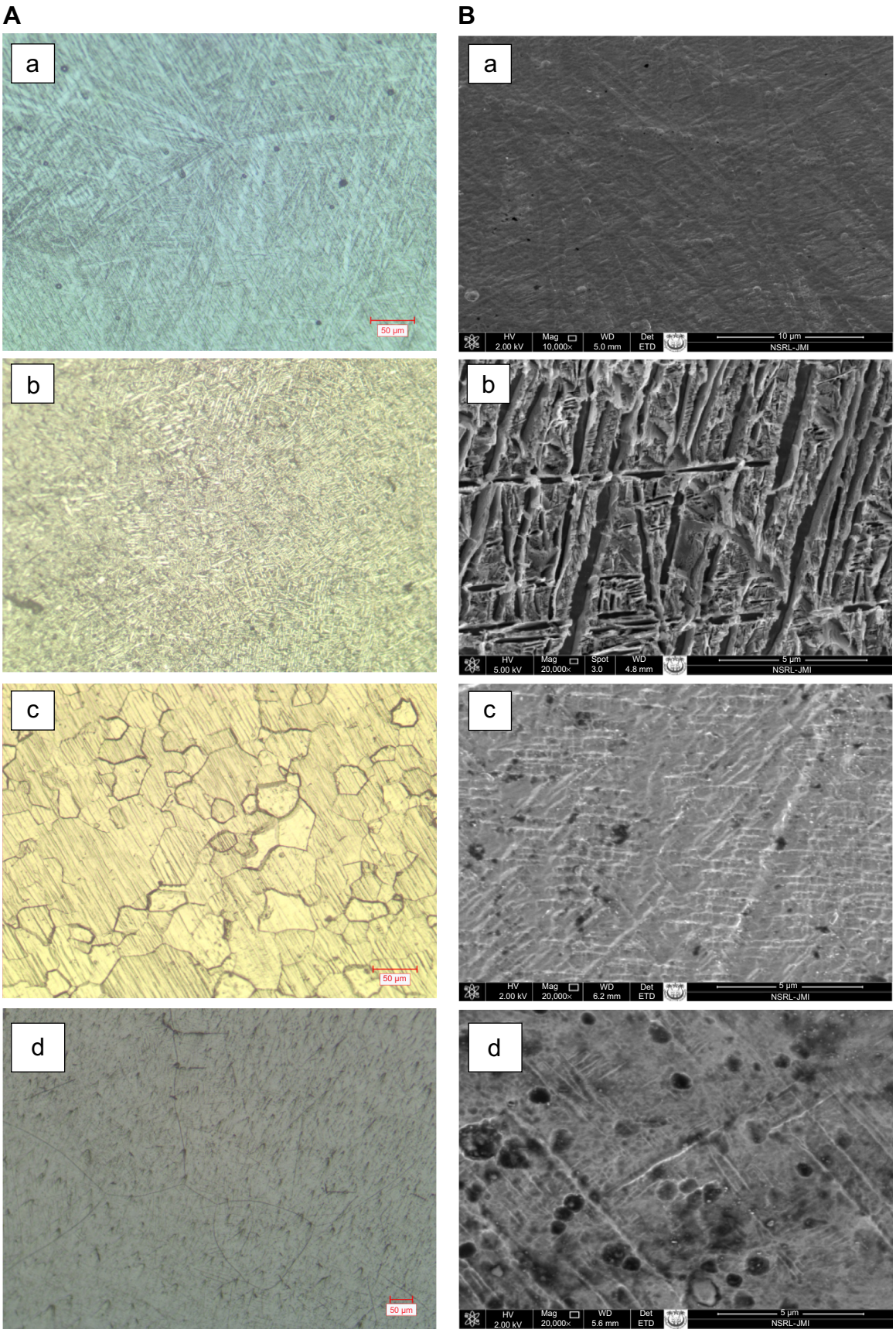

Figure 3 (*Continued*)

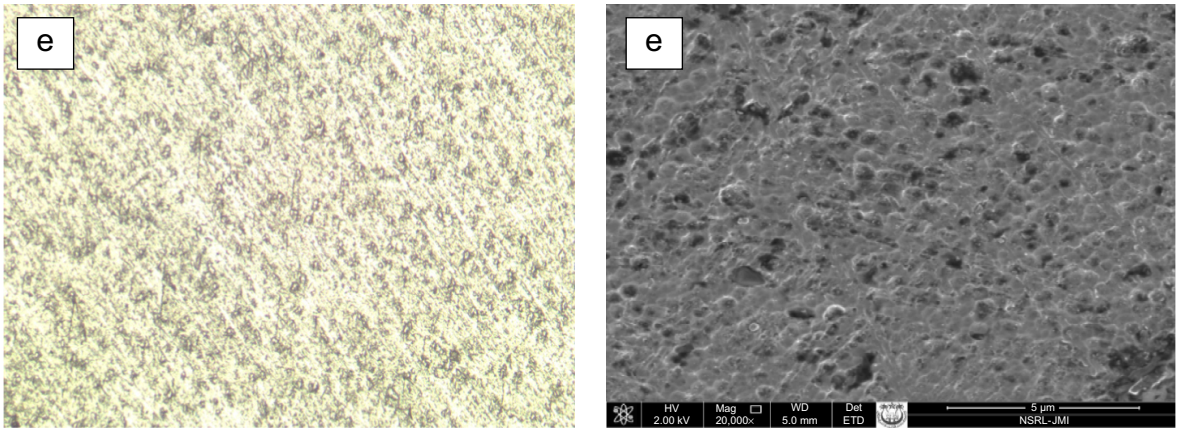

Figure 3 Microstructural investigations by (**A**) optical microscopy and (**B**) scanning electron microscopy of the Ti-20.6Nb-13.6Zr-0.5V alloy samples: (a) as-cast, and deformed at 850°C and solution-treated for 1 hour at same temperature followed by (b) furnace-cooling, (c) air-cooling, (d) water-quenching, and (e) aging of water-quenching samples at 500°C for 5 hours.

Mechanical properties

Microhardness

The effect of thermal treatment on the microhardness of the TNZV samples is presented in Figure 5A, which shows that the AC samples have a higher HV than the FC and WQ samples because of the formation of fine phases. In contrast, the WQ sample showed a significant decrease in hardness (HV 220±3), as reported by others.[44] Consequently, it is expected that the presence of martensite with an insufficient amount of α in the microstructure would decrease the HV after WQ from 850°C. However, aging treatment of the WQ samples increased the HV significantly, and this thermal treatment provided the most hardness (HV 292±5). Many authors[8,34,51,52] have mentioned that substantial enhancement in hardness can be achieved after aging treatment. This heat treatment process has the ability to precipitate a fine α phase in the matrix by decomposition of martensite and retained β phases. These fine precipitates of α in the matrix increases the HV of the TNZV alloy. Thus, the HV of the aged samples was higher when fine α-grains were crystallized in the β-matrix.

Elastic modulus

The elastic modulus is strongly influenced by the bonding force among atoms, the phase/crystal structure,[11] and the chemical composition of a Ti material.[20,53] Therefore, in any multiphase Ti alloy, the specific modulus of the phases and their volume fractions are key parameters for developing the modulus. It is well known that all these parameters depend mainly on the

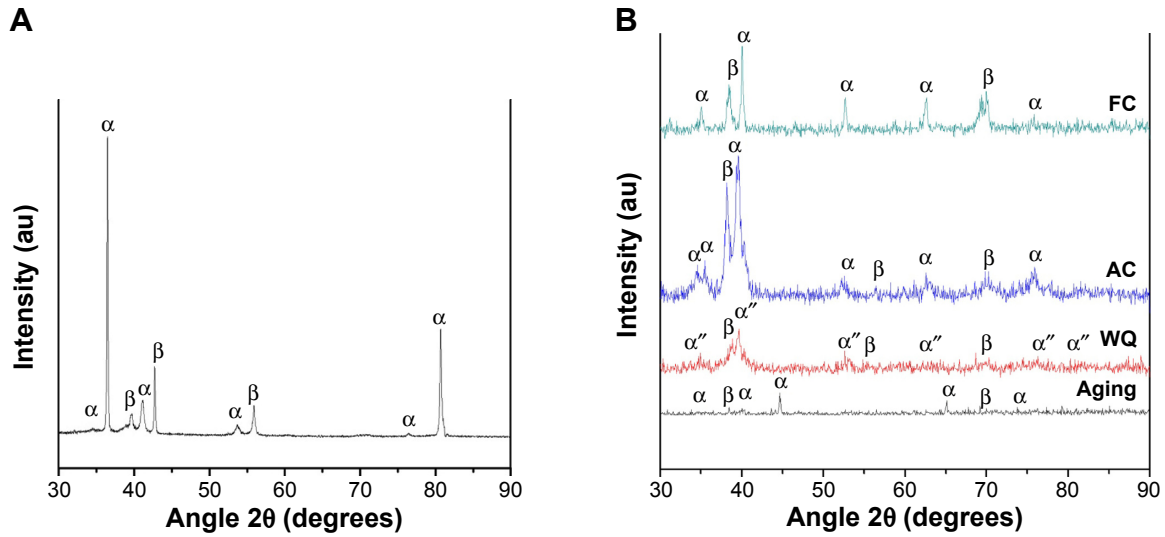

Figure 4 X-ray diffraction profiles of (**A**) as-cast TNZV alloy and (**B**) TNZV alloy samples deformed at 850°C and solution treated for 1 hour at the same temperature followed by WQ, AC, FC, and aging of water-quenched samples at 500°C for 5 hours.
Abbreviations: TNZV, Ti-20.6Nb-13.6Zr-0.5V; AC, air-cooling; FC, furnace-cooling; WQ, water-quenching.

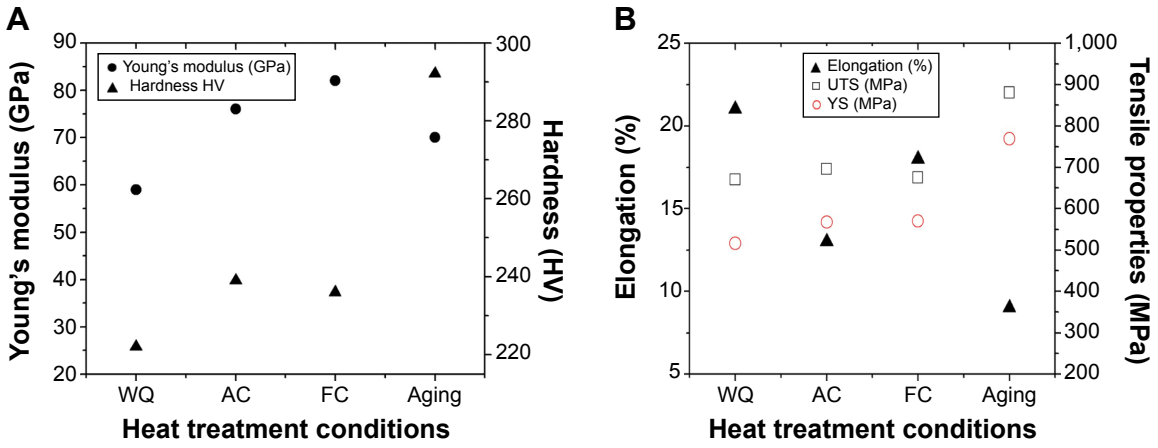

Figure 5 (**A**) Hardness and elastic modulus and (**B**) tensile results of TNZV alloy deformed at 850°C and solution treated at 850°C for 1 hour followed by WQ, AC, FC, and aging of water-quenched samples at 500°C for 5 hours.
Abbreviations: TNZV, Ti-20.6Nb-13.6Zr-0.5V; AC, air-cooling; FC, furnace-cooling; WQ, water-quenching; UTS, ultimate tensile strength; YS, off-set yield strength.

history of thermal and TMP.[54] The literature reports that the elastic modulus of the phases in Ti alloys increases in the sequence $E\beta < E\alpha'' < E\alpha < E\omega$.[11,20,44,55] It is inferred that the microstructure of Ti materials has a significant effect in reducing the modulus, because a mixture of β and α″ phases lowers the modulus whereas the α phase increases it.[20,56] The modulus of TNZV subjected to the different thermal treatment conditions is shown in Figure 5A, which indicates that the modulus of the thermal-treated TNZV samples varies from 59 to 82 GPa. It can be seen that the modulus decreases significantly with increasing cooling rate. After solutionizing at 850°C, the WQ samples developed a microstructure consisting of martensite and retained β phase (Figure 3Ad and Bd). Given that both these phases afford a lower elastic modulus as compared with α phase, the WQ samples had the lowest modulus value (59±1.9 GPa) when compared with the FC and AC samples. On the other hand, compared with the AC samples, the FC samples had a higher amount of α because of the slower cooling rate. Therefore, the high modulus value of the FC samples is associated with the maximum volume fraction of α phase in the microstructure. It was observed that aging treatment resulted in decomposition of the low modulus martensite and retained β phase into high modulus α. The modulus of the aged samples increased to 70±2.3 GPa.

Tensile properties

Tensile test results were obtained for the TNZV samples deformed at 850°C and solution treated at the same temperature followed by WQ, AC, and FC. The YS, UTS, and fracture plasticity (e%) of the samples is shown in Figure 5B, which demonstrate that the UTS, YS, and e% varied from 670 to 696 MPa, 516 to 570 MPa, and 13% to 21%, respectively. It can be seen that the strength of the AC samples is higher than that of the FC or WQ samples. The superior strength of the AC samples is a result of the fine microstructure produced by relatively rapid cooling. In addition, the YS of the FC and AC samples were analogous and higher than that of the WQ samples. On the other hand, the WQ samples showed remarkable ductility (21%) compared with FC or AC samples. The solid solution-hardening effect after WQ is the main factor of the reasonable strength. However, formation of soft β and α″ martensite phases in the microstructure of WQ samples played an important role in producing a lower YS and better e%. Hao et al[44] pointed out that the martensite structure has lower strength and HV but better e%, which is in good agreement with the present tensile strength result of WQ samples.

The UTS, YS, and e% of the WQ samples after aging treatment were found to be 880 MPa, 769 MPa, and 9%, respectively. These values suggest that the strength (UTS and YS) of the aged samples was significantly higher than the strength of other the heat-treated samples but the ductility was substantially lower. Thus, the extensive increase in strength after aging can be related to the precipitation of fine α phase in the matrix as a result of decomposition of martensite and retained β phases. On the other hand, the lowered e% of the aged samples is related to the precipitation of fine α particles along the pre-existing martensite plates, which act as effective sites for nucleation of the cracks, and in turn, decrease the e% of the alloy.

Electrochemical properties

Open circuit potential

Figure 6 shows the variation in OCP of TNZV alloy in different conditions as a function of immersion time in naturally aerated Ringer's solution at 37°C, until its variation with

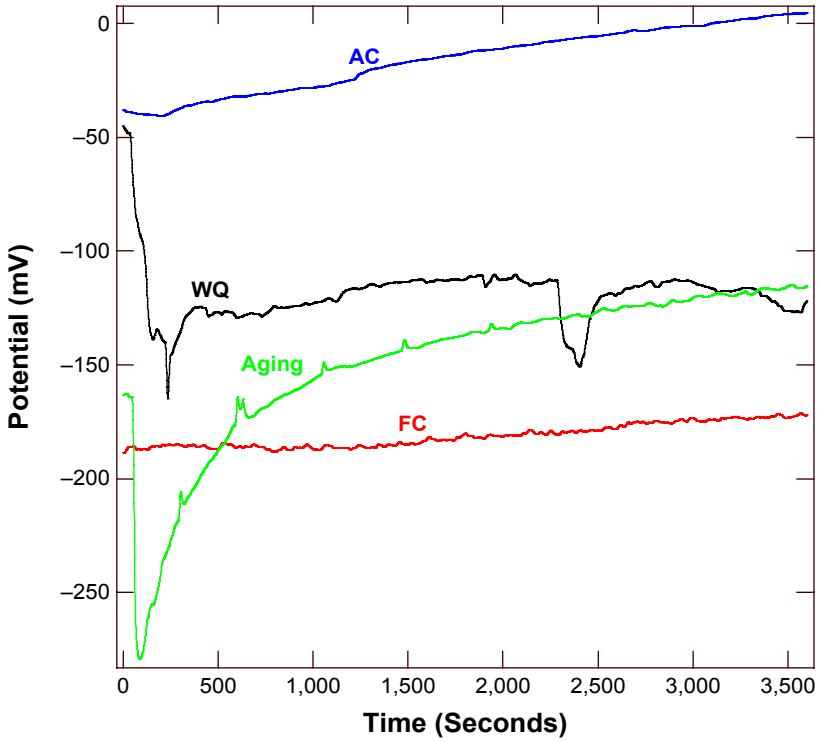

Figure 6 Open-circuit potential versus time curves of the TNZV alloy in Ringer's solution at 37°C deformed at 850°C and solution treated at the same temperature for 1 hour followed by WQ, AC, FC, and aging of water-quenched samples at 500°C for 5 hours.
Abbreviations: TNZV, Ti-20.6Nb-13.6Zr-0.5V; AC, air-cooling; FC, furnace-cooling; WQ, water-quenching.

time became negligible. The steady-state OCP of TNZV alloy varies with heat treatment conditions. By comparing the results depicted in Figure 6, it can be observed that the AC samples have more positive corrosion potential values (nobler behavior) than the FC, WQ, and aged samples. In this research, of all the thermally treated samples, the FC samples showed a greatest decrease in OCP. In addition, the OCP curve for the WQ and aged samples shows fluctuations in the initial stages and then becomes stable, whereas the AC and FC samples showed a tendency for spontaneous formation of surface oxides and a continuous shift in a noble (positive) direction when they were in contact with Ringer's solution. The time profiles for OCP are characteristic of passive film formation, especially in the stabilized region, on the alloy surfaces immersed in aerated solutions under different heat treatment conditions.[57] AC samples, however, showed the greatest tendency for spontaneous formation of oxide film in Ringer's solution. The OCP values for all heat treatment conditions show an overall increase with the time duration of 1 hour, indicating that their resistance to corrosion increases with time and reaches a relatively stable value. In other words, the OCP shifts in the positive direction, indicating passive formation of a protective oxide film on the surface of the TNZV alloy.

The protective film forms rapidly and acts as a barrier to metal dissolution, leading to a decrease in the corrosion rate. The thickness of the spontaneously formed protective oxide film on the surfaces of Ti and its alloys has been reported to be 1–4 nm under open circuit conditions.[58] It is well known that the superior corrosion behavior of Ti and its alloys is attributable to spontaneous creation of a tightly adherent protective oxide film on their surface, even in solutions with a low oxygen content.[59] Oliveira et al[60] reported creation of an oxide film on Ti-13Zr-13Nb and Ti-50Zr alloys in aerated solution. It has been reported in the literature that X-ray photoelectron spectroscopy reveals that the amorphous oxide film formed comprises three types of oxides, ie, TiO, Ti_2O_3, and TiO_2.[18,61,62] It has also been found that oxides of Ti, TiO, and Ti_2O_3, transform to more stable TiO_2 and come out on the electrode/electrolyte interface after direct contact between Ti material and the electrolyte.[26] TiO_2 is an n-type semiconductor,[63] and the corrosion of Ti is controlled kinetically by migration of oxygen vacancies through this film.[64] Hence, the corrosion behavior reached a relatively stable state as the resistance to corrosion of the electrode improved. The decrease in anodic dissolution current of the Ti alloy and shifting the OCP gradually in the positive direction are normal results of an increase in corrosion resistance.

It is important to mention that many researchers[57,65–67] have found that the film formed on the surface of Ti and its alloys in various physiological solutions shows a two-layered structure comprising a dense inner layer and a porous outer layer. The excellent corrosion behavior of the Ti-Nb-Zr alloy system is essentially because of the barrier provided by the inner layer, which offers high resistance.[57,65]

Many authors[61,68–71] have reported that the passive film in the Ti-Nb-Zr alloy system consists principally of TiO_2 with trace quantities of Nb_2O_5 and ZrO_2. The presence of Nb_2O_5 or ZrO_2 with the main passive TiO_2 layer develops the structural integrity of the oxide film and increases its resistance to dissolution.[61,72] For example, the presence of Nb cations enhances the passivation properties of the surface film by decreasing the concentration of anion vacancies present on a Ti oxide film. These anion vacancies are generated by the presence of lower Ti oxidation states.[40,61,73]

Potentiodynamic polarization

Figure 7 shows the potentiodynamic anodic polarization curves for different heat-treated TNZV samples as measured with respect to a saturated calomel electrode in naturally aerated Ringer's solution at 37°C. The continuity, stability, and intensity of the passive Ti oxide film are analyzed by this technique. As can be seen from Figure 7, the polarization curves obtained for the investigated TNZV alloy samples in all heat treatment conditions show a typical active-passive characterization, a rising anodic current with increasing potential, and then transforming directly into the passive area from the Tafel curves. The average E_{corr} values can be estimated from these curves as –181.18, –191.81, –125.81, –209.23 mV (versus the saturated calomel electrode) for the FC, AC, WQ, and aged samples, respectively. The corrosion potentials determined from the polarization curves are significantly lower than those obtained from the open circuit potential measurements. This is expected, as the polarization tests were started at a cathodic potential relative to the corrosion potential, so the surface passive oxide film was at least partially removed owing to the highly reducing initial potentials.

The mean I_{corr} and corrosion rates were obtained for the TNZV alloy by the Tafel extrapolation analysis method using both anodic and cathodic branches of the polarization curves (Figure 8). The corresponding corrosion data, which include the mean corrosion current densities (I_{corr}), corrosion potentials (E_{corr}), and corrosion rates of TNZV alloy under different thermal treatment conditions, are given in Table 2.

From the corrosion test results presented in Table 2, it can be observed that in most of the heat treatment conditions, the E_{corr} varies roughly within a narrow range. It can be seen that the FC samples and AC samples show almost comparable E_{corr} values. On the other hand, aging of the WQ samples results in a further decrease in the E_{corr} value, which

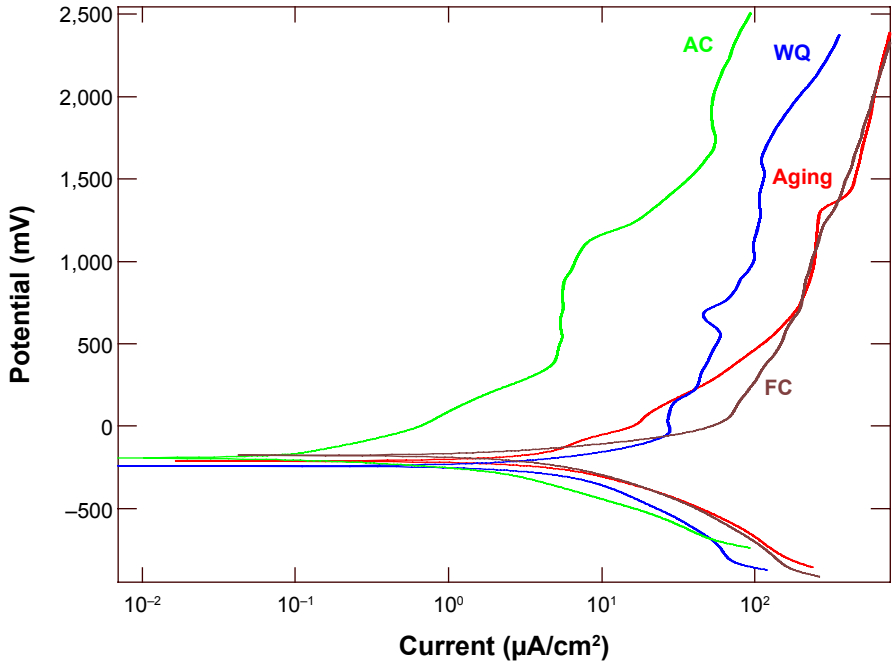

Figure 7 Cyclic polarization of the TNZV alloy in a Ringer's solution at 37°C deformed at 850°C and solution treated at same temperature for 1 hour followed by WQ, AC, FC, and aging of WQ samples at 500°C for 5 hours.
Abbreviations: TNZV, Ti-20.6Nb-13.6Zr-0.5V; AC, air-cooling; FC, furnace-cooling; WQ, water-quenching.

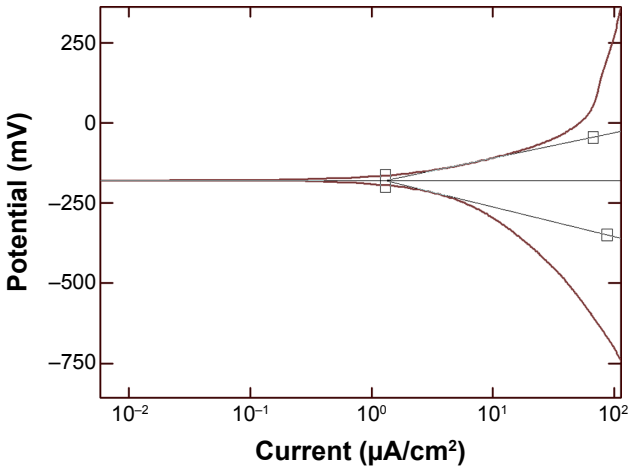

Figure 8 Tafel plots obtained for furnace-cooled sample in Ringer's solution at 37°C.

is lower than that of the FC, AC, or WQ samples. Comparing the four anodic curves, however, it can be noticed that the FC samples and aged samples exhibit similar anodic polarization behaviors, including almost comparable current densities of 4.508 and 5.7645 μA/cm^2, respectively, at approximately 2,500 mV (Ag/AgCl). As mentioned in the OCP analysis, as soon as the TNZV samples are rinsed in Ringer's solution, a protective surface oxide film is formed on the surface of the samples and they become passivated, which is reproduced in the anodic polarization curves (Figure 7).

The corrosion current density of the WQ samples lies between the values for the AC and FC samples. Moreover, the anodic current densities are lower for the AC samples than for the FC, WQ, and aged samples. This indicates that, of all the samples, the minimum I_{corr} is for the AC samples due to the more compact and protective nature of the surface film formed on the AC samples. This implies that the anodic current density of TNZV under all thermal treatment conditions increases with an increase in the potential, but this increase is always larger for the FC samples and aged samples. The rise in I_{corr} with the potential is likely to be because of the unsatisfactory increase in oxide film thickness, to recompensate the increase in potential. It is reported that this increase in current could be associated with the oxidation of TiO and Ti_2O_3 to TiO_2.[61] Thus, it appears that the surface oxide films become thick to compensate for the increase in potential where the current does not change with potential.

Table 2 Results of electrochemical tests via anodic polarization curves for the heat-treated Ti-20.6Nb-13.6Zr-0.5V alloy samples in Ringer's solution at 37°C

Cooling conditions	E_{corr} (mV)	I_{corr} (μA/cm^2)	Corrosion rate (mils/year)
WQ	−125.81	2.2246	1.81
AC	−191.81	1.0324	0.84
FC	−181.18	4.508	3.67
Aging	−209.23	5.7645	4.51

Abbreviations: E_{corr}, corrosion potential; I_{corr}, passive current density; WQ, water-quenched; AC, air-cooled; FC, furnace-cooled.

In the current research, it is expected that the fine (α+β) structure in the matrix of the AC samples increases the α/β interface area and then accelerates the galvanic corrosion of the alloy. Regardless of this, the AC samples exhibited a lower I_{corr} and a lower corrosion rate than the FC or aged samples. It has been found that the corrosion behavior of cp-Ti (single α phase) is lower than that of Ti-6Al-7Nb alloy (α+β).[74] Therefore, the most likely reason for the better corrosion behavior of the AC samples is the presence of a small amount of less noble α phase in their microstructures. During the diffusionless martensitic β→α″ phase transformation in the WQ samples, the solute partitioning does not occur and, consequently, the WQ samples have improved corrosion stability (lower I_{corr}) as a result of the formation of a more stable passive film than the FC or aged samples. This result agrees well with the result reported in the literature[66] and confirms that the β ST WQ Ti-13Nb-13Zr alloy remains passive in Ringer's solution at positive potentials as 2.5 V (saturated calomel electrode). On the other hand, formation of martensite occurred in the WQ samples via a shear mechanism of phase transformation, that involves an invariant plane strain shape deformation with a large shear component. This entails a high amount of strain energy because the shape change must be accommodated in the parent phase.[31,75] Therefore, in spite of the absence of any α/β interface in the WQ samples, their corrosion behavior was found to be less stable than that of the AC samples (Figures 6 and 7) due to the presence of a strained and highly faulted substructure.

Aging of the WQ samples created higher amounts of fine precipitates of less noble α phase in the microstructure, as shown in Figure 3Ae and Be. Thus, in the same way, the α/β interface increased with the increase in α phase volume friction, which in turn led to a decrease in E_{corr} (−209.23 mV) and an increase in I_{corr} (5.7645 μA/cm^2) despite relieving the strain energy associated with martensite.

Conclusion

The effect of TMP on the microstructure, mechanical properties, and electrochemical behavior of metastable β Ti-20.6Zr-13.6Nb-0.5 V alloy for biomedical applications has been investigated. Based on the results of the present study, the following conclusions are drawn. A wide range of microstructures with varying distributions

and morphologies of elongated/equiaxed α, β phases, or martensite is attained depending upon the TMP conditions. AC samples show greater hardness (HV) and strength (UTS, YS) as compared with FC or WQ samples. WQ samples offer reasonable strength and higher plasticity (21%) compared with other heat-treated samples. WQ samples introduce a lower Young's modulus (59±1.9 GPa) compared with other heat-treated samples due to the martensitic transformations. Aging treatment of WQ samples causes an increase in the HV, strength, and elastic modulus, and also a decrease in the e%, owing to decomposition of martensite and retained β in α phase. Corrosion tests indicated that the TNZV alloy undergoes spontaneous passivation owing to spontaneously formed oxide film in the environment of the human body. The AC samples had a lower corrosion rate owing to their fine grain size and higher HV than the samples treated under other conditions. The AC samples, which had optimum results for strength and resistance to corrosion as well as reasonable results for e% and modulus, can be considered as a potential candidate for biomedical application after further investigations on in vitro and in vivo behavior. The TNZV alloy developed in the present study has superior mechanical properties and corrosion behavior, but further studies on the tribological and biocompatibility behavior of the alloy are needed to assess its overall potential for biomedical application.

Acknowledgments

The authors are grateful to the Ministry of High Education and Scientific Research, Iraq, for its financial assistance with this work, and to the Defense Metallurgical and Research Laboratories in Hyderabad, India, for manufacturing the titanium alloy.

Disclosure

The authors report no conflicts of interest in this work.

References

1. Wang K. The use of titanium for medical applications in the USA. *Mater Sci Eng A.* 1996;213:134–137.
2. Boehlert CJ. Microstructure, creep, and tensile behavior of a Ti-12-Al-38Nb (at.%) beta and orthorhombic alloy. *Mater Sci Eng A*. 1999; 267:82–98.
3. Niinomi M. Recent research and development in titanium alloys for biomedical applications and healthcare goods. *Sci Technol Adv Mater*. 2003;4:445–454.
4. Mythili R, Thomas Paul V, Saroja S, et al. Study of transformation behavior in Ti-4.4Ta-1.9Nb alloy. *Mater Sci Eng A*. 2005;390:299–312.
5. Niinomi M. Fatigue performance and cytotoxicity of low rigidity titanium alloy, Ti-29Nb-13Ta-4.6Zr. *Biomaterials*. 2003;24: 2673–2683.
6. Yu J, Zhao ZJ, Li LX. Corrosion fatigue resistances of surgical implant stainless steel and titanium alloys. *Corros Sci.* 1993;35:587–597.
7. Okazaki Y, Ito Y, Kyo K, et al. Corrosion resistance and corrosion fatigue strength of new titanium alloys for medical implants without V and Al. *Mater Sci Eng A Struct Mater*. 1996;213:138–147.
8. Lkeda M, Komatsu SY, Sowa I, et al. Aging behavior of the Ti-29Nb-13Ta-4.6Zr new beta alloy for medical implants. *Metall Mater Trans A*. 2002;33:487–493.
9. Sumner D, Galante J. Determinants of stress shielding: design versus materials versus interface. *Clin Orthop Relat Res.* 1992;274:202–212.
10. Gasser B. [*Design and Engineering Criteria for Titanium Devices, Titanium in Medicine*]. Berlin, Germany: Springer; 2001. German.
11. Ho WF, Ju CP, Lin JH. Structure and properties of cast binary Ti-Mo alloys. *Biomaterials*. 1999;20:2115–2122.
12. Park CH, Park JW, Yeom JT, et al. Enhanced mechanical compatibility of submicrocrystalline Ti-13Nb-13Zr alloy. *Mater Sci Eng A*. 2010;527:4914–4919.
13. Long M, Rack HJ. Titanium alloys in total joint replacement – a materials science perspective. *Biomaterials*. 1998;19:1621–1639.
14. Nang S, Banerjee R, Stechschulte J, et al. Comparison of microstructural evolution in Ti-Mo-Zr-Fe and Ti-15Mo biocompatible alloys. *J Mater Sci Mater Med*. 2005;16:679–685.
15. Niinomi M. Recent metallic materials for biomedical applications. *Metall Mater Trans A.* 2002;33A:477–486.
16. Ikehata H, Nagasako N, Furuta T, et al. First-principles calculations for development of low elastic modulus Ti alloys. *Phys Rev B Condens Matter.* 2004;70:174113–174118.
17. Abdel-Hady M, Hinoshitaa K, Morinagaa M. General approach to phase stability and elastic properties of β-type Ti alloys using electronic parameters. *Scr Mater*. 2006;55:477–480.
18. Been J, Grauman JS. Titanium and titanium alloys. In: Revie RW, editor. *Uhlig's Corrosion Handbook*. 2nd ed. New York, NY, USA: John & Wiley Inc; 2000.
19. Niinomi M. Mechanical properties of biomedical titanium alloys. *Mater Sci Eng A*. 1998;243:231–236.
20. Collings EW. *Physical Metallurgy of Titanium Alloys*. Metals Park, OH, USA: ASM International; 1984.
21. Niinomi M, Akahori T, Takeuchi T, et al. Mechanical properties and cytotoxicity of new beta type titanium alloy with low melting points for dental applications. *Mater Sci Eng C*. 2005;25:417–425.
22. Zhang RG, Acoff VL. Processing sheet materials by accumulative roll bonding and reaction annealing from Ti/Al/Nb elemental foils. *Mater Sci Eng A*. 2007;463:67–73.
23. Tang X, Ahmed T, Rack HJ. Phase transformations in Ti-Nb-Ta and Ti-Nb-Ta-Zr alloys. *J Mater Sci.* 2000;35:1805–1811.
24. Ribeiro AL, Junior RC, Cardoso FF, Filho RB, Vaz LG. Mechanical, physical, and chemical characterization of Ti-35Nb-5Zr and Ti-35Nb-10Zr casting alloys. *J Mater Sci Mater Med*. 2009;20:1629–1636.
25. Kim JI, Kim HY, Inamura T, et al. Shape memory characteristics of Ti-22Nb-(2-8)Zr (at.%) biomedical alloys. *Mater Sci Eng A*. 2005;403: 334–339.
26. Sun F, Hao YL, Nowak S, et al. A thermo-mechanical treatment to improve the superelastic performances of biomedical Ti-26Nb and Ti-20Nb-6Zr (at.%) alloys. *J Mech Behav Biomed Mater*. 2011;4:1864–1872.
27. Yang G, Zhang T. Phase transformation and mechanical properties of the $Ti_{50}Zr_{30}Nb_{10}Ta_{10}$ alloy with low modulus and biocompatible. *J Alloys Compd.* 2005;392:291–294.
28. Degarmo PE, Black JT, Kohser RA. *Materials and Processes in Manufacturing*. 9th ed. New York, NY, USA: Wiley; 2003.
29. Weaver ML, Garmestani H. Microstructures and mechanical properties of commercial titanium foils processed via the melt overflow process *Mater Sci Eng A*. 1998;247:229–238.
30. Bache MR, Evans WJ. Impact of texture on mechanical properties in an advanced titanium alloy *Mater Sci Eng A.* 2001;319–321:409–414.
31. Lonardelli I, Gey N, Wenk HR, et al. In situ observation of texture evolution during $\alpha \rightarrow \beta$ and $\beta \rightarrow \alpha$ phase transformations in titanium alloys investigated by neutron diffraction. *Acta Mater*. 2007;55:5718–5727.

32. Ding R, Guo ZX, Wilson A. Microstructural evolution of a Ti6-Al-4V alloy during thermomechanical processing. *Mater Sci Eng A*. 2002;327:233–245.
33. Geetha M, Mudali UK, Gogia AK, et al. Influence of microstructure and alloying elements on corrosion behavior of Ti-13Nb-13Zr alloy. *Corros Sci*. 2004;46:877–892.
34. Majumdar P, Singh SB, Chakraborty M. The role of heat treatment on microstructure and mechanical properties of Ti-13Zr-13Nb alloy for biomedical load bearing applications. *J Mech Behav Biomed Mater*. 2011;4:1132–1144.
35. Majumdar P, Singh SB, Chatterjee UK, et al. Corrosion behaviour of heat treated boron free and boron containing Ti-13Zr-13Nb (wt%) alloy in simulated body fluid. *J Mater Sci Mater Med.* 2011;22:797–807.
36. Kuhn H, Medlin D. *Metals Handbook. Volume 8, Mechanical Testing and Evaluation*. Materials Park, OH, USA: ASM International; 1972.
37. Gonzalez EG, Mirza-Rosca JC. Study of the corrosion behaviour of titanium and some of its alloys for biomedical and dental applications. *J Electroanal Chem*. 1999;471:109–112.
38. Oliveira NT, Biaggio SR, Rocha-Filho RC, Bocchi N. Electrochemical studies on zirconium and its biocompatible alloys Ti-50Zr at.% and Zr-2.5Nb wt% in simulated physiologic media. *J Biomed Mater Res A*. 2005;74:397–407.
39. Cremasco A, Osorio WR, Freire CMA, et al. Electrochemical corrosion behaviour of a Ti–35Nb alloy for medical prostheses. *Electrochim Acta*. 2008;53:4867–4874.
40. Rosalbino F, Maccio D, Scavino G, et al. In vitro corrosion behaviour of Ti-Nb-Sn shape memory alloys in Ringer's physiological solution. *J Mater Sci Mater Med*. 2012;23:865–871.
41. Banumathy S, Prasad KS, Mandal RK, et al. Effect of thermomechanical processing on evolution of various phases in Ti-Nb alloys. *Bull Mater Sci*. 2011;34:1421–1434.
42. Boyer R, Welsch G, Collings EW. *Materials Properties Hand Book: Titanium Alloys.* 1st ed. Materials Park, OH, USA; ASM International; 1994.
43. Ahmed T, Rack HJ. Martensitic transformations in Ti-(16–26 at%) Nb alloys. *J Mater Sci*. 1996;31:4267–4276.
44. Hao YL, Niinomi M, Kuroda D, et al. Young's modulus and mechanical properties of Ti-29Nb-13Ta-4.6Zr in relation to α″ martensite. *Metall Mater Trans A*. 2002;33:3137–3144.
45. Mantani Y, Tajima M. Phase transformation of quenched α″ martensite by aging in Ti–Nb alloys. *Mater Sci Eng A*. 2006;438–440:315–319.
46. Lee T, Heo Y-U, Lee CS. Microstructure tailoring to enhance strength and ductility in Ti-13Nb-13Zr for biomedical application. *Scr Mater*. 2013;69:785–788.
47. Moffat D, Larbalestier D. The competition between martensite and omega in quenched Ti-Nb alloys. *Metall Mater Trans A*. 1988;19:1677–1686.
48. Geetha M, Singh AK, Muraleedharan K, et al. Effect of thermomechanical processing on microstructure of a Ti-13Nb-13Zr alloy. *J Alloys Compd.* 2001;329:264–271.
49. Banumathy S, Mandal RK, Singh AK. Structure of orthorhombic martensitic phase in binary Ti–Nb alloys. *J Appl Phys.* 2009;106:093518.
50. Murakami Y. Review phase transformations and heat treatment. In: Kumura H, Izumi O, editors. *Titanium 80. Science and Technology, Proceedings of the 4th International Conference on Titanium*. New York, NY, USA: Science and Technology, Metallurgical Society of AIME; 1980.
51. Kuroda D, Kawasaki H, Yamamoto A, et al. Mechanical properties and microstructures of new Ti-Fe-Ta and Ti-Fe-Ta-Zr system alloys. *Mater Sci Eng C.* 2005;25:312–320.
52. Slokar J, Matkovic T, Matkovic P. Alloy design and property evaluation of new Ti-Cr-Nb alloys. *Mater Des*. 2012;33:26–30.
53. Song Y, Xu DS, Yang R, et al. Theoretical study of the effects of alloying elements on the strength and modulus of β-type bio-titanium alloys. *Mater Sci Eng A.* 1999;260:269–274.
54. Lee YT, Welsch G. Young modulus and damping of Ti-6Al-4V alloy as a function of heat treatment and oxygen content. *Mater Sci Eng A*. 1990;128:77–89.
55. Majumdar P, Singh SB, Chakraborty M. Elastic modulus of biomedical titanium alloys by nano-indentation and ultrasonic techniques – a comparative study. *Mater Sci Eng A*. 2008;489:419–425.
56. Cui WF, Guo AH. Microstructures and properties of biomedical TiNbZrFe titanium alloy under aging conditions. *Mater Sci Eng A.* 2009;527:258–262.
57. Robin A, Carvalho OAS, Schneider SG, et al. Corrosion behavior of Ti-xNb-13Zr alloys in Ringer's solution. *Mater Corros.* 2008;59:929–933.
58. Marino CEB, Oliveira EM, Rocha-Filho RC, et al. On the stability of thin-anodic-oxide films of titanium in acid phosphoric media. *Corros Sci.* 2001;43:1465–1476.
59. Okazaki Y, Tateishi T, Ito Y. Corrosion resistance of implants alloys in pseudo physiological solution and role of alloying elements in passive films. *Mater Trans JIM.* 1997;38:78–84.
60. Oliveira NTC, Ferreira EA, Duarte LT, Biaggio SR, Rocha-Filho RC, Bocchi N. Corrosion resistance of anodic oxides on the Ti–50Zr and Ti-13Zr-13Nb alloys. *Electrochim Acta*. 2006;51:2068–2075.
61. Yu SY, Scully JR. Corrosion and passivity of Ti-13Nb-13Zr in comparison to other biomedical implant alloys. *Corrosion*. 1997;53:965–976.
62. Pouilleau J, Devilliers D, Garrido F, et al. Structure and composition of passive titanium oxide films. *Mater Sci Eng B*. 1997;47:235–243.
63. Pan J, Leygraf C, Thierry D, et al. Corrosion resistance for biomaterial applications of TiO2 films deposited on titanium and stainless steel by ion-beam-assisted sputtering. *J Biomed Mater Res.* 1997;35:309–318.
64. Hong SB, Eliaz N, Sachs EM, et al. Corrosion behavior of advanced titanium-based alloys made by three-dimensional printing (3DP™) for biomedical applications. *Corros Sci.* 2001;43:1781–1791.
65. Assis SL, Costa I. Electrochemical evaluation of Ti-13Nb-13Zr, Ti-6Al-4V and Ti-6Al-7Nb alloys for biomedical application by long-term immersion tests. *Mater Corros.* 2007;58:329–333.
66. Assis SL, Wolynec S, Costa I. The electrochemical behaviour of Ti-13Nb-13Zr alloy in various solutions. *Mater Corros*. 2008;59:739–743.
67. Alves VA, Reis RQ, Santos ICB, et al. In situ impedance spectroscopy study of the electrochemical corrosion of Ti and Ti-6Al-4V in simulated body fluid at 25°C and 37°C. *Corros Sci.* 2009;51:2473–2482.
68. Manivasagam G, Mudali UK, Asokamani R, et al. Corrosion and microstructural aspects of titanium and its alloys as orthopaedic devices. *Corros Rev*. 2003;21:125–159.
69. Choubey A, Basu B, Balasubramaniam R. Electrochemical behavior of Ti based alloys in simulated human body fluid environment. *Trends Biomater Artif Organs*. 2005;18:64–72.
70. Li J, Zhou L, Li Z. Corrosion behavior of a new titanium alloy TZNT for surgical implant application in Ringer's solution. *Rare Metals*. 2010;29:37–44.
71. Bai Y, Li SJ, Prima F, et al. Electrochemical corrosion behavior of Ti-24Nb-4Zr-8Sn alloy in a simulated physiological environment. *Appl Surf Sci.* 2012;258:4035–4040.
72. Geetha M, Singh AK, Asokamani R, et al. Ti based biomaterials, the ultimate choice for orthopaedic implants – a review. *Prog Mater Sci*. 2009;54:397–425.
73. Metikoš-Hukovic´M, Kwokal A, Piljac J. The influence of niobium and vanadium on passivity of titanium-based implants in physiological solution. *Biomaterials.* 2003;24:3765–3775.
74. Raman V, Tamilselvi S, Nanjundan S, et al. Electrochemical behaviour of titanium and titanium alloy in artificial saliva. *Trends Biomater Artif Organs*. 2005;18:137–140.
75. Wayman CM, Bhadeshia HKDH. Phase transformations, nondiffusive. In: Cahn RW, Haasen P, editors. *Physical Metallurgy*. Amsterdam, The Netherlands: Elsevier Science Publishers; 1996.